Magneto-optical Selection Rules in Bilayer Bernal Graphene

Yen-Hung Ho,[†,‡] Yu-Huang Chiu,[†,*] De-Hone Lin,[‡] Chen-Peng Chang,[§] and Ming-Fa Lin[†,*]

[†]Department of Physics, National Cheng Kung University, Tainan, Taiwan 701, [‡]Department of Physics, National Sun Yat-Sen University, Kaohsiung, Taiwan 804, and [§]Center of General Education, National Tainan University of Technology, Tainan, Taiwan 710

ARTICLE

ABSTRACT The low-frequency magneto-optical properties of bilayer Bernal graphene are studied by the tight-binding model with the four most important interlayer interactions taken into account. Since the main features of the wave functions are well-depicted, the Landau levels can be divided into two groups based on the characteristics of the wave functions. These Landau levels lead to four categories of absorption peaks in the optical absorption spectra. Such absorption peaks own complex optical selection rules, and these rules can be reasonably explained by the characteristics of the wave functions. In addition, twin-peak structures, regular frequency-dependent absorption rates, and complex field-dependent frequencies are also obtained in this work. The main features of the absorption peaks are very different from those in monolayer graphene and have their origin in the interlayer interactions.

KEYWORDS: graphene · Landau level · optical absorption · selection rule · magnetic field · tight-binding model

Ever since few-layer graphenes (FLGs) were first produced by mechanical exfoliation[1,2] and thermal decomposition,[3,4] they have attracted considerable experimental and theoretical research because of their exotic physical properties resulting from the hexagonal structure. Monolayer graphene (MG) and bilayer Bernal graphene (BBG; AB-stacked bilayer graphene), two of the simplest few-layer graphenes, display very different electronic structures. MG exhibits isotropic linear bands near the Fermi level ($E_F = 0$); these bands become gradually anisotropic parabolic bands as the energy exceeds the region of ± 0.5 eV.[5] In BBG, the linear bands change into two pairs of parabolic bands due to the present interlayer interactions and stacking configurations.[6−14] Each pair comprises the occupied valence and unoccupied conduction bands, which are asymmetric about E_F.[6,9] The conduction and valence bands of the first pair slightly overlap about E_F, while those of the second pair rise at the energies[12] of 0.34 eV ($\simeq \gamma_1 + \gamma_6$) and -0.39 eV ($\simeq -\gamma_1 + \gamma_6$), respectively, where γ_s's[8,10,15−17] ($s = 1$, 3, 4, and 6) are four important interlayer interactions in BBG. The unusual electronic structures of MG and BBG have been experimentally verified through angular-resolved photoemission spectroscopy.[18,19] The main features of the zero-field energy bands (*e.g.*, the broken linear dispersions in MG and the two groups of asymmetric electronic states in BBG) should be reflected in the features of the Landau levels (LLs) resulting from the magnetic fields.[12]

In the presence of a uniform perpendicular magnetic field, $\mathbf{B} = B_0\hat{z}$, the zero-field energy bands of FLGs become the dispersionless LLs. Some magneto-electronic properties of FLGs have been obtained by measurements of the quantum Hall conductivity,[2,20−22] scanning tunneling spectroscopy,[22−24] and cyclotron resonance.[25,26] The effective mass (EM) approximation and the tight-binding (TB) model, two theoretical methods based on different concepts in calculations, are usually utilized to study the magneto-optical properties of layered-graphene systems. In MG, EM shows that the linear bands become LLs characterized by the special relation $E_n^{c,v} \propto (n^{c,v}B_0)^{1/2}$,[27,28] where c (v) is the index of the conduction (valence) bands. $E_n^{c,v}$ and $n^{c,v}$ are the energy and the integer quantum number of the nth energy band, respectively. However, TB indicates that the special relation will be broken as the energy exceeds the region of ± 0.5 eV because the linear dispersions become gradually parabolic as energy exceeds this region.[29] As for the optical absorption spectra, the low-frequency absorption peaks possess the selection rule $|\Delta n| = |n^c - n^v| = 1$, and their frequency is proportional to $\sqrt{B_0}$,[30] which has been confirmed by magneto-transmission measurements.[25,31,32]

*Address correspondence to airegg.py90g@nctu.edu.tw, mflin@mail.ncku.edu.tw.

Received for review October 31, 2009 and accepted February 12, 2010.

Published online February 24, 2010. 10.1021/nn9015339

For BBG, EM takes the LL structures of MG and uses them in the BBG calculations. Interlayer interactions are regarded as perturbations (EM considers only one or two interlayer interactions). On the basis of EM calculations, the first theoretical study[13] of LLs in BBG derived an effective two-dimensional Hamiltonian that describes the low-energy electronic excitations. Furthermore, EM predicts the existence of two groups of the occupied and unoccupied LLs, and they are symmetric about E_F because the parabolic bands at $B_0 = 0$ are symmetric in the calculations.[30,33,34] The low-energy LLs in their results follow the relation $E_n^{c,v} \propto B_0$.[30] As for the optical absorption spectra, EM calculations show that there are three categories of absorption peaks.[30] The absorption frequencies obey a linear function of B_0 in weak fields and depend linearly on $\sqrt{B_0}$ as the corresponding energy leaves the parabolic band region.[30] The three categories own the same optical selection rule $|\Delta n| = 1$.[14,30,35,36] In TB, a magnetic field and the four most important interlayer interactions[8,12,13] are simultaneously included in the calculations. The magnetic flux ϕ through a hexagon corresponding to the strongest field strength (~60 T) in experiments is much smaller than the flux quantum ϕ_0 ($\phi \sim \phi_0/1320$). From the viewpoint of the TB perturbation theory, electronic states that lie in close proximity to each other at $B_0 = 0$ will be aggregated and become dispersionless LLs under the influence of a magnetic field. The characteristics of electronic states at $B_0 = 0$ are directly reflected in the main features of LLs. The interlayer interactions strongly affect the electronic properties, especially for low-energy levels. These interactions are neither negligible nor suitable as perturbations. TB indicates that the low-energy LLs should exhibit more complex features;[12] that is, there exists an energy gap, two groups of asymmetric LLs (^{1st}LL^{c,v}s and ^{2nd}LL^{c,v}s), and no simple relations between $E_n^{c,v}$ and B_0. The main features would be reflected in the magneto-optical properties.

In the initial stage of our work in studying the magneto-electronic properties, only eigenvalues and eigenvectors at strong magnetic field strength were obtained[37] because the Hamiltonian matrix is quite large; for example, the matrix is about 31 600 × 31 600 for MG at 10 T. Through the band-like matrix strategy[12,38−42] designed by our group, the eigenvalues and the wave functions at weak fields (~1 T) are thus clearly depicted.[12] However, the calculation of optical properties is more complex and time-consuming than that of the electronic properties because detailed calculations for a huge velocity matrix and reliable characterization of the wave functions are necessary for the TB-based optical absorption spectra. In this work, the localized features of the wave functions are utilized to effectively reduce the computation time, and thus the optical absorption spectra can be solved. It is the first time that the optical properties of BBG calculated by TB are obtained. The influence of the four most important interlayer interactions on the magneto-optical absorption spectra of BBG is investigated in detail by TB and gradient approximation.[37,40−44] The wave functions are clearly depicted and used to divide the LLs into two groups,[12] ^{1st}LLs and ^{2nd}LLs. The two groups lead to four categories of optical absorption peaks. These peaks exhibit twin-peak structures, complex selection rules, regular frequency-dependent absorption rates, and complicated field-dependent absorption frequencies. What deserves to be mentioned is that our study is more complete in nature, and the presented results are more reliable than those of previous works. Previously, experimental and theoretical research mainly focused on the optical properties associated with ^{1st}LLs. However, in our work, the optical absorption peaks resulting from both groups are discussed in detail, and each peak can be clearly identified. A detailed comparison of optical absorption spectra between MG and BBG is made. In addition, comparisons of optical properties between AA-stacked bilayer graphene (AABG) and BBG and between EM and TB are also made.

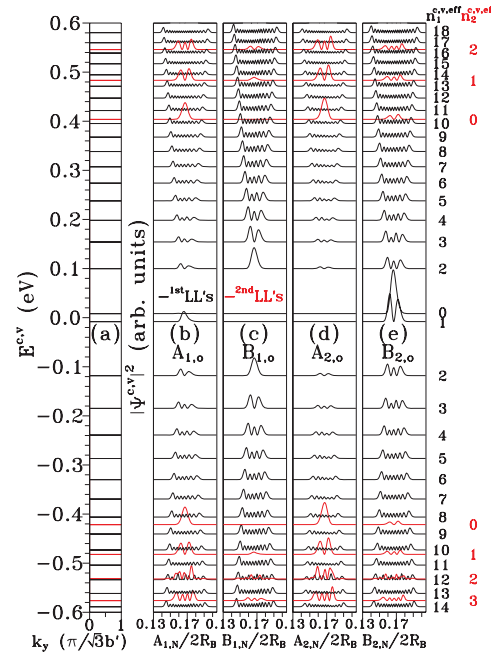

Figure 1. (a) Landau levels of bilayer Bernal graphene at B_0 = 40 T. The wave functions of (b) $A_{1,o}$, (c) $B_{1,o}$, (d) $A_{2,o}$, and (e) $B_{2,o}$ atoms with odd integer indices shown.

RESULTS AND DISCUSSION

The dispersionless LLs of BBG at $B_0 = 40$ T are shown in Figure 1a. The interlayer interactions strongly influence the main features of LLs. The conduction and valence bands are asymmetric. There is an energy gap between the lowest unoccupied LL and the highest occupied LL. On the basis of the characteristics of wave functions, LLs can be classified into two groups, ^{1st}LLs (black curves) and ^{2nd}LLs (red curves). ^{1st}LLs appear at $|E^{c,v}| > 0$, and ^{2nd}LLs begin at $E^c \gtrsim \gamma_1 + \gamma_6$ (0.34 eV) and $E^v \lesssim -\gamma_1 + \gamma_6$ (−0.39 eV). The onset energies of the first and second groups are consistent with those of the

first and second pairs in the zero-field sub-bands. Furthermore, no simple relation between the energy and field strength can be found for these LLs; that is, $E_n^{c,v}$ is not directly proportional to either B_0 or $\sqrt{B_0}$.[12]

The characteristics of the wave functions deserve a closer investigation because they strongly dominate the optical properties. Each LL is composed of four-fold degenerate states with similar characteristics. At $k_x = k_y = 0$, the wave functions mainly consist of four localized sub-envelope functions centered at positions $x_1 = 1/6$, $x_2 = 1/3$, $x_3 = 2/3$, and $x_4 = 5/6$; $x_{j=1-4} = A_{i,N}/2R_B$ or $= B_{i,N}/2R_B$. $A_{i,N}$ ($B_{i,N}$) indicates the Nth A (B) atom on the ith layer, where $N = 1, 2 \ldots 2R_B$ and $i = 1, 2$ denote the atomic site in the primitive unit cell and the layer index, respectively (please see the detailed discussion regarding these representations in the Methods). The feature of a wave function resulting from the atoms with an even number ($A_{i,e}^{c,v}$ and $B_{i,e}^{c,v}$) is similar to that with an odd ($A_{i,o}^{c,v}$ and $B_{i,o}^{c,v}$) number, where e (o) is an even (odd) integer. Because of this, only odd atoms are discussed in the following calculations. For convenience, one of the four-fold degenerate states at $x_1 = 1/6$ is selected to be examined, as shown in Figure 1b−e. Through appropriate fitting, the wave functions of the n_1th [1st]LL (black curves) and n_2th [2nd]LL (red curves) can be expressed as

$$A_{1,o}^{c},A_{2,o}^{c} \propto \varphi_2(x),B_{1,o}^{c} \propto \varphi_1(x),B_{2,o}^{c} \propto \varphi_0(x),n_1^{c,\mathrm{eff}} = 0 \text{ for } n_1 = 1 \quad (1a)$$

$$A_{1,o}^{v},A_{2,o}^{v} \propto \varphi_0(x),B_{1,o}^{v} \propto \varphi_2(x),B_{2,o}^{v} \propto \varphi_1(x),n_1^{v,\mathrm{eff}} = 1 \text{ for } n_1 = 1 \quad (1b)$$

$$A_{1,o}^{c,v},A_{2,o}^{c,v} \propto \varphi_{n_1-1}(x),B_{1,o}^{c,v} \propto \varphi_{n_1-2}(x),B_{2,o}^{c,v} \propto \varphi_{n_1}(x) \text{ for } n_1^{c,v,\mathrm{eff}} = n_1 \geq 2 \quad (1c)$$

$$A_{1,o}^{c,v},A_{2,o}^{c,v} \propto \varphi_0(x),B_{1,o}^{c,v} \propto \varphi_2(x),B_{2,o}^{c,v} \propto \varphi_1(x),n_2^{c,v,\mathrm{eff}} = 0 \text{ for } n_2 = 1 \quad (2a)$$

$$A_{1,o}^{c,v},A_{2,o}^{c,v} \propto \varphi_{n_2-1}(x),B_{1,o}^{c,v} \propto \varphi_{n_2-2}(x),B_{2,o}^{c,v} \propto \varphi_{n_2}(x) \text{ for } n_2^{c,v,\mathrm{eff}} = n_2 - 1 \geq 1 \quad (2b)$$

$\varphi_n(x)$ is the product of the nth order Hermite polynomial and Gaussian function,[12,29,40] where n is the number of zero points of $\varphi_n(x)$ and chosen to define the quantum number of a LL.[12] That is to say, there are four quantum numbers in each LL because a LL wave function is made up of four magnetic TB functions. Thus, an effective quantum number, n^{eff}, defined by one of these four quantum numbers is necessary to identify each LL. The effective quantum number of a LL in each group is assigned by the number of zero points in one of the four magnetic TB functions, with the largest amplitude among these four TB functions at the onset energy of each group. Accordingly, $n_1^{c,v,\mathrm{eff}}$ ($n_2^{c,v,\mathrm{eff}}$) is the effective quantum number of the [1st]LLs ([2nd]LLs) defined by the quantum number of $B_{2,o}^{c,v}$ ($A_{1,o}^{c,v}$). It should be noted that the wave functions of two groups are composed of not only the B atoms but also the A atoms, which are different from those calculated by EM, including only contributions from the B atoms.[13,14] Such difference could cause the optical properties obtained by TB and EM to exhibit different features. [1st]LLs and [2nd]LLs can be distinguished by the different features of the wave functions in the mixed region ($E^c \gtrsim 0.34$ eV and $E^v \lesssim -0.39$ eV), which is useful in analyzing the optical excitation channels.

When BBG is subjected to an electromagnetic field at zero temperature, only excitations from the occupied to the unoccupied bands occur. On the basis of Fermi's golden rule, the optical absorption function is given by

$$A(\omega) \propto \sum_{n_{1,2}^{c,\mathrm{eff}},n_{1,2}^{v,\mathrm{eff}}} \int_{1\mathrm{st\ BZ}} \frac{d\mathbf{k}}{(2\pi)^2} \left| \langle \psi^c(n_{1,2}^{c,\mathrm{eff}},\mathbf{k}) \times \left| \frac{\hat{\mathbf{E}}\cdot\mathbf{P}}{m_e} \right| \psi^v(n_{1,2}^{v,\mathrm{eff}},\mathbf{k}) \rangle \right|^2 \times \mathrm{Im} \left\{ \frac{f[E^c(\mathbf{k},n_{1,2}^{c,\mathrm{eff}})] - f[E^v(\mathbf{k},n_{1,2}^{v,\mathrm{eff}})]}{E^c(\mathbf{k},n_{1,2}^{c,\mathrm{eff}}) - E^v(\mathbf{k},n_{1,2}^{v,\mathrm{eff}}) - \omega - i\Gamma} \right\} \quad (3)$$

where $\hat{\mathbf{E}}$ is the unit vector of an electric polarization. Γ (=1 meV) is a broadening parameter and often affected by temperature and defect effects. If a purer sample is manufactured and its physical properties are observed under a sufficiently low temperature, Γ will be small enough for observing important fine structures.[22,45] Furthermore, $\langle \psi^c(n_{1,2}^c,\mathbf{k})|\hat{\mathbf{E}}\cdot\mathbf{P}/m_e|\psi^v(n_{1,2}^v,\mathbf{k})\rangle$ is the velocity matrix element derived from the dipole transition and denoted M^{cv}. In this work, M^{cv} is calculated by gradient approximation. Through detailed calculations, M^{cv} can be simplified to be the product of three matrices, the initial state (occupied state, ψ^v), the final state (unoccupied state, ψ^c), and $\nabla_k H_{ij}$. The last term corresponds to the direction of electric polarization; that is, it is $\partial H_{ij}/\partial k_x$ for polarization along the x-axis in this work. The elements of $\partial H_{ij}/\partial k_x$ are nonzero only for H_{ij} associated with the hopping integrals, as are the velocity matrix elements. In other words, when the velocity matrix element does not vanish, the initial and final states in the product should be the two states corresponding to the nonvanishing hopping integrals. Accordingly, M^{cv} is expressed as

$$\left\{ \sum_{i=1,2} \sum_{N,N'=1}^{2R_B} [(A_{io}^c + A_{ie}^c)^* \times (B_{io'}^v + B_{ie'}^v)] \nabla_k \langle A_{i,N\mathbf{k}}|H_B|B_{i,N'\mathbf{k}}\rangle + \sum_{i,j=1,2;i\neq j} \sum_{N,N'=1}^{2R_B} [(B_{io}^c + B_{ie}^c)^* \times (B_{jo'}^v + B_{je'}^v)] \nabla_k \langle B_{i,N\mathbf{k}}|H_B|B_{j,N'\mathbf{k}}\rangle + \sum_{i,j=1,2;i\neq j} \sum_{N,N'=1}^{2R_B} [(B_{io}^c + B_{ie}^c)^* \times (A_{jo}^v + A_{je'}^v)] \nabla_k \langle B_{i,N\mathbf{k}}|H_B|A_{j,N'\mathbf{k}}\rangle \right\} + hc \quad (4)$$

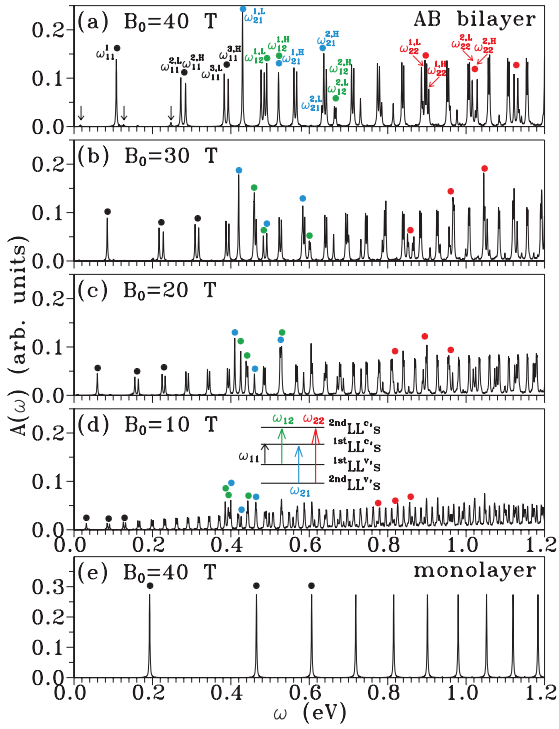

Figure 2. Optical absorption spectra of bilayer Bernal graphene at (a) 40, (b) 30, (c) 20, and (d) 10 T. The spectrum of monolayer graphene at 40 T is plotted in (e).

The first, second, and third terms in eq 4 correspond to the three hopping integrals γ_0, γ_3, and γ_4, respectively. That is to say, the optical excitations are provided by the three channels related to γ_0, γ_3, and γ_4. For convenience, $(A^c_{io} + A^c_{ie})^* \times (B^v_{io'} + B^v_{ie'})$, $(B^c_{io} + B^c_{ie})^* \times (B^v_{jo'} + B^v_{je'})$, and $(B^c_{io} + B^c_{ie})^* \times (A^v_{jo'} + A^v_{je'})$ are represented by $M^{cv}_{AB}(\gamma_0)$, $M^{cv}_{BB}(\gamma_3)$, and $M^{cv}_{BA}(\gamma_4)$, respectively, in the following discussions. It should be noted that eq 4 implies that the characteristics of the wave functions would play a dominant role in determining the selection rule and absorption rate in optical excitations.

The low-frequency optical absorption spectra of BBG regarding four different magnetic field strengths are shown in Figure 2a−d. The absorption spectrum of MG is also shown in Figure 2e. In Figure 2a, the absorption spectrum of BBG at $B_0 = 40$ T presents prominent and inconspicuous (indicated by the black arrows) peaks. The prominent peaks with definite optical selection rules are discussed in detail in the following paragraphs. The peaks can mainly be classified into four categories of peaks, ω_{11} (black dots), ω_{22} (red dots), ω_{12} (green dots), and ω_{21} (blue dots), which originate in the four different excitation channels, $^{1st}LL^v$ to $^{1st}LL^c$, $^{2nd}LL^v$ to $^{2nd}LL^c$, $^{1st}LL^v$ to $^{2nd}LL^c$, and $^{2nd}LL^v$ to $^{1st}LL^c$, respectively. The former (latter) two channels result from the transitions between two LLs in the same (different) groups, as illustrated by the inset of Figure 2d, and they display obvious optical selection rules.

The optical excitations associated with each prominent peak can clearly be identified, as shown in Figure 2a. For convenience, the excitations of ω_{11}, ω_{22}, ω_{12}, and ω_{21} are, respectively, represented as $n^{v,eff}_1 \rightarrow n^{c,eff}_1$, $n^{v,eff}_2 \rightarrow n^{c,eff}_2$, $n^{v,eff}_1 \rightarrow n^{c,eff}_2$, and $n^{v,eff}_2 \rightarrow n^{c,eff}_1$ in the following. The selection rule of ω_{ij} is denoted by Δn_{ij} $(= n^{c,eff}_j - n^{v,eff}_i)$. As to ω_{11} and ω_{22}, only the first peak (ω^1_{11}) of ω_{11} originates in single channel $1 \rightarrow 2$. The other mth peak ω^m_{11} (ω^m_{22}) consists of the pair $\omega^{m,L}_{11}$ and $\omega^{m,H}_{11}$ $(\omega^{m,L}_{22}$ and $\omega^{m,H}_{22})$ corresponding to $m \rightarrow m + 1$ and $m + 1 \rightarrow m$ $(m - 1 \rightarrow m$ and $m \rightarrow m - 1)$, respectively. The superscript L (H) indicates the lower (higher) energy of the pair. For example, ω^2_{11} (ω^1_{22}) is composed of $\omega^{2,L}_{11}$ and $\omega^{2,H}_{11}$ $(\omega^{1,L}_{22}$ and $\omega^{1,H}_{22})$ owing to $2 \rightarrow 3$ and $3 \rightarrow 2$ $(0 \rightarrow 1$ and $1 \rightarrow 0)$, respectively. The origin of a twin-peak structure is that the energies of $m \rightarrow m + 1$ $(m - 1 \rightarrow m)$ and $m + 1 \rightarrow m$ $(m \rightarrow m - 1)$ in ω_{11} (ω_{22}) are slightly different owing to the asymmetry of the occupied and unoccupied LLs. It should be noted that similar twin-peak structures are also shown in a recent experiment conducted to study the magneto-absorption spectra.[45] In short, the optical selection rules of ω_{11} and ω_{22} can be represented by $\Delta n_{11} = \Delta n_{22} = \pm 1$, which is the same as the LLs in MG.

As for the intergroup transitions, twin-peak structures are also obtained in ω_{12} and ω_{21}. The mth peak of ω_{12} is formed with the pair, $\omega^{m,L}_{12}$ originating in $m \rightarrow m$ and $\omega^{m,H}_{12}$ resulting from $m + 1 \rightarrow m - 1$. For instance, the first pair is indicated by $\omega^{1,L}_{12}$ and $\omega^{1,H}_{12}$ in Figure 2a, which correspond to $1 \rightarrow 1$ and $2 \rightarrow 0$, respectively. That is to say, $\omega^{m,L}_{12}$ owns the optical selection rule $\Delta n_{12} = 0$ and $\omega^{m,H}_{12}$ possesses $\Delta n_{12} = -2$. For ω_{21}, the excitations $0 \rightarrow 0$ and $0 \rightarrow 2$ lead to the peaks $\omega^{1,L}_{21}$ and $\omega^{1,H}_{21}$ of the first pair in Figure 2a, respectively. The other channels $m - 1 \rightarrow m + 1$ and $m \rightarrow m$ result in the pair $\omega^{m,L}_{21}$ and $\omega^{m,H}_{21}$, respectively. In other words, the selection rules of ω_{21} are $\Delta n_{21} = 0$ and $\Delta n_{21} = 2$. Obviously, the optical selection rules of ω_{12} and ω_{21} are different from those of ω_{11} and ω_{22}, a fact which is not clearly discussed in previous theoretical works.

The optical selection rules can be explained from two different aspects, that is, the effective quantum numbers and the numbers of zero points between the initial and final states. Both aspects are based on the premise that the velocity matrix is derived from the dipole transition. The product of the conduction and valence wave functions in eq 4 would not only determine the allowed excitation channel but also enable us to estimate the absorption rate. This means that the dissimilarities in selection rules of the four categories mainly result from the characteristics of the wave functions. In eq 4, $M^{cv}_{AB}(\gamma_0)$ associated with γ_0 dominates the excitations of the prominent peaks. It strongly depends on the numbers of zero points of $A^{c,v}_1$ and $B^{c,v}_1$ $(A^{c,v}_2$ and $B^{c,v}_2)$ since $M^{cv}_{AB}(\gamma_0) = (A^c_{io} + A^c_{ie})^* \times (B^v_{io'} + B^v_{ie'})$. $M^{cv}_{AB}(\gamma_0)$ has nonzero values only when $A^{c,v}_1$ and $B^{c,v}_1$ $(A^{c,v}_2$ and $B^{c,v}_2)$ own the same $\varphi_n(x)$ because of the orthogonality of $\varphi_n(x)$. Thus, the selection rules of prominent peaks can be easily obtained by the definition of the wave functions in eqs 1 and 2. From the aspect of the numbers of zero

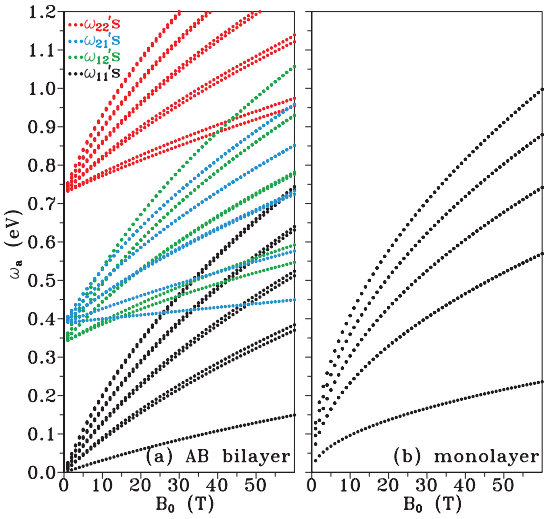

Figure 3. Field-dependent optical absorption frequencies of (a) bilayer Bernal graphene and (b) of monolayer graphene.

points between $A_i^{c,v}$ and $B_i^{c,v}$, these states own the same number of zero points in an available excitation channel in both intragroup and intergroup transitions. As for the effective quantum numbers, the selection rules are $\Delta n_{11} = \Delta n_{22} = \pm 1$, $\Delta n_{12} = 0, -2$, and $\Delta n_{21} = 0, 2$. Although these selection rules are different, all excitations obey the underlying condition that the numbers of zero points of the initial and final states in the dipole-transition-derived velocity matrix are the same.

In addition to the optical selection rules, the peak intensity and absorption frequency are also discussed in this work. The absorption rate significantly relies on the field strength and the excitation energy. In Figure 2a−d, the peak intensity is increased with enlarging field strength, while the opposite is true for the peak number. The peak intensity under a fixed magnetic field strength is determined by the product of two wave functions with respect to the two nearest-neighbor atoms. The wave functions of ^{1st}LLs (^{2nd}LLs) are mainly dominated by the *B* (*A*) atoms. The amplitudes of $A_i^{c,v}$ and $B_i^{c,v}$, respectively, gradually grow and decrease (decrease and grow) with increasing energy in ^{1st}LLs (^{2nd}LLs). Accordingly, the value of the product of $A_i^{c,v}$ and $B_i^{c,v}$ increases (decreases) with rising energy for ω_{11} and ω_{22} (ω_{12} and ω_{21}). This value is largest when the amplitudes of $A_i^{c,v}$ and $B_i^{c,v}$ are equal. The intensities of ω_{11} and ω_{22} (ω_{12} and ω_{21}) thus increase (decline) with increasing frequency. Furthermore, some peaks with commensurate energies overlap because the peak spacing declines as the frequency increases; this overlap is responsible for the variation in peak intensity. In contrast to BBG, MG exhibits absorption peaks with uniform intensity (Figure 2e).

The field-dependent absorption frequencies (ω_a) of ω_{11}, ω_{22}, ω_{12}, and ω_{21} are shown in Figure 3a by the black, red, green, and blue dots, respectively. The ω_a of the four categories rises with increasing B_0. These absorption frequencies do not exhibit the simple relations indicated by EM calculations;[29] that is, the frequencies are not directly proportional to either B_0 or $\sqrt{B_0}$. Apparently, $\omega_a \propto \sqrt{B_0}$ in MG (Figure 3b) is very different from that in BBG. The main reason for the difference between BBG and MG is that interlayer interactions play important roles in BBG and are not negligible in calculations. In addition, the convergent frequencies of ω_{11}, ω_{22}, ω_{12}, and ω_{21} at the weak field strength are approximately 0 eV, 0.73 eV ($2\gamma_1$), 0.34 eV ($\gamma_1 + \gamma_6$), and 0.39 eV ($\gamma_1 - \gamma_6$), respectively. This implies that the optical measurements can reasonably determine the values of γ_1 and γ_6 through observing the convergent frequencies of absorption peaks. The predicted results are very useful and reliable for experimental studies.

The inconspicuous peaks indicated by arrows in Figure 2a also obey specific selection rules (not shown). These peaks mainly originate from excitations related to two interlayer interactions (γ_3 and γ_4) and differ from the prominent peaks associated with the intralayer hopping integral (γ_0). The inconspicuous peak intensities are much weaker than the intensities of the prominent peaks because the values of the velocity matrix elements corresponding to γ_3 and γ_4 are much smaller than those related to γ_0. The different origins and selection rules of the prominent and inconspicuous peaks imply that the optical properties cannot be simply derived from the eigenenergies of LLs. The detailed calculations of the velocity matrix and reliable characterization of the wave functions are necessary to determine the optical selection rules and the peak intensity.

The atomic hopping integrals are important to analyze the physical properties of BBG. So far, the values of these atomic interactions have not been well-defined. Figure 4a is the optical absorption spectrum calculated with the parameters used in our work.[8] Panels b−d in Figure 4 are the results calculated with three other sets of parameters[10,16,17] used in the investigations of BBG. The optical absorption spectra corresponding to the four sets of parameters show similar qualitative properties; that is, they exhibit four categories of absorption peaks, twin-peak structures, and the same optical selection rules. However, the absorption frequencies in the four results are slightly different because the values of the four sets of parameters are distinct. The reliability of these parameters could be verified through more accurate experimental measurements with a purer bilayer graphene.

TB and EM methods are based on different concepts in the BBG calculations. The former simultaneously includes a magnetic field and four important interlayer interactions in the calculations. However, the latter takes the LL structures of MG to study the physical properties of BBG, where interlayer interactions are regarded as perturbations. The wave functions in TB calculations are well-characterized and different from those in EM calculations. The magneto-optical absorp-

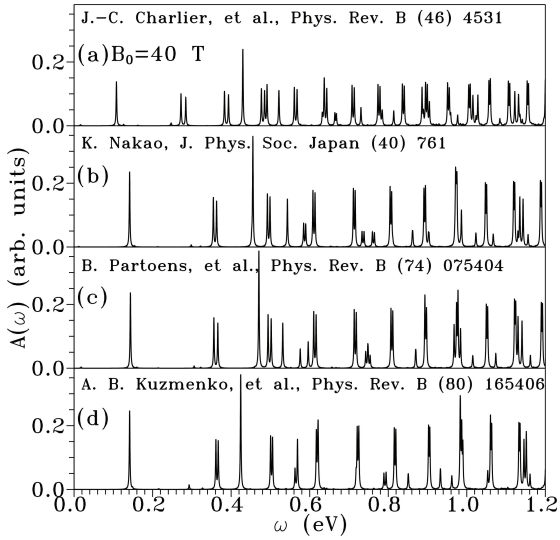

Figure 4. (a) Optical absorption spectra at $B_0 = 40$ T calculated with the parameters used in our work. (b−d) Results calculated with three other sets of parameters commonly used in the investigations of bilayer Bernal graphene.

tion spectra studied by TB and EM exhibit five crucial differences. The former demonstrate four categories of absorption peaks, twin-peak structures in each category, complex optical selection rules, and complex field-dependent absorption frequencies. However, the latter display three peak categories, no twin-peak structure, a single selection rule, and the simple field-dependent absorption frequencies $\omega_a \propto B_0$ and $\omega_a \propto \sqrt{B_0}$. Moreover, the regular frequency-dependent peak intensities are shown in TB results, while they are not obtained in EM results. These differences mainly originate from the different concepts and distinct definitions of the wave functions in the two methods.

In addition to BBG, AABG also presents special optical properties, as shown in Figures S6 and S7 of the Supporting Information. AABG and BBG show similar LL features, that is, two groups of LLs and an asymmetric

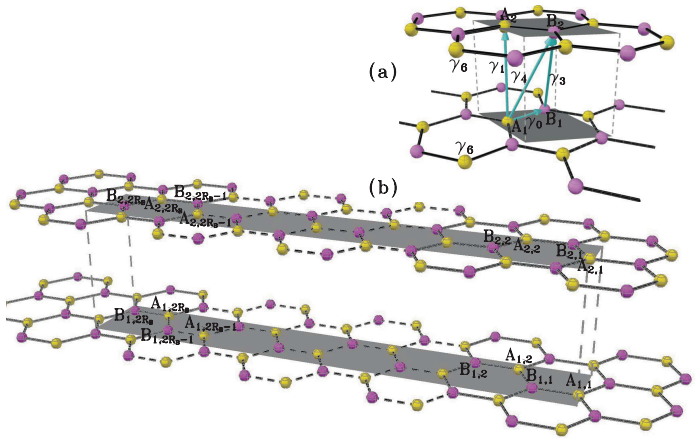

Figure 5. Primitive unit cells of bilayer Bernal graphene in the (a) absence and (b) presence of a magnetic field; γ_0 (2.598 eV) is the nearest-neighbor hopping integral, and the four important interlayer interactions are γ_1 (0.364 eV), γ_3 (0.319 eV), γ_4 (0.177 eV), and γ_6 (−0.026 eV).

structure. However, these two bilayer graphenes display different optical properties. AABG contains two categories of absorption peaks resulting from the intragroup excitations, and these peaks exhibit only one single optical selection rule. No twin-peak structure similar to that in the BBG case arises from the special relations in the two LL groups of AABG. The differences of the optical absorption spectra of AABG and BBG imply that the optical properties cannot be directly identified through only the eigenvalues of LLs. An explicit analysis of the characteristics of the wave functions and detailed calculations of the velocity matrix elements are necessary to calculate the optical properties. Both the magneto-electronic and magneto-optical properties of AABG and BBG reflect the main features of zero-field electronic and optical properties. A detailed analysis of the magneto-optical absorption spectra in AABG is discussed in an unpublished work.[46]

TB is widely applied to tackle physical problems of semiconductors and carbon-related systems. Through the strategy developed by our group, the complex Hamiltonian matrix can be solved. The eigenvalues and wave functions are clearly depicted in this calculation and thus can be used to interpret the results in optical properties. Because TB calculations simultaneously include the magnetic field and the important interlayer interactions, such results are more reliable and accurate over a much wider frequency range. Besides, TB can conceivably be expanded to investigate other layered-graphene systems (multilayer graphenes and bulk graphite) and other physical properties (electronic excitations and transport properties).

SUMMARY AND CONCLUSIONS

In summary, it can be said that the interlayer interactions play very important roles in the magneto-optical properties of BBG. In this work, detailed calculations of the velocity matrix and reliable characterization of the wave functions are provided for analyzing the optical properties. On the basis of the characteristics of the wave functions, the asymmetric LLs can be divided into two groups. These two groups lead to four categories of prominent optical absorption peaks: ω_{11}, ω_{22}, ω_{12}, and ω_{21}. Each category exhibits twin-peak structures originating from the asymmetry of LLs. The optical selection rules of the four categories are $\Delta n_{11} = \pm 1$, $\Delta n_{22} = \pm 1$, $\Delta n_{12} = 0, -2$, and $\Delta n_{21} = 0, 2$, respectively. All of the selection rules can be reasonably explained by the characteristics of the wave functions. The peak intensities of ω_{11} and ω_{22} (ω_{12} and ω_{21}) increase (decrease) with rising frequency. The field-dependent absorption frequencies are not directly proportional to either B_0 or $\sqrt{B_0}$. Furthermore, the convergent absorption frequencies at the weak field strength might be helpful and reliable in determining the interlayer atomic interactions γ_1 and γ_6. The main results of BBG in this work are more complex in nature than those of MG and different from

those in previously published works studied by EM. The above-mentioned magneto-optical properties could be confirmed by magneto-absorption spectroscopy measurements.[26,31,32]

METHODS

The optical absorption spectrum is calculated by gradient approximation based on the tight-binding model. The geometric configuration of a primitive unit cell in BBG is shown in Figure 5a. The unit cell includes four sublattices, A_1, B_1, A_2, and B_2. The subscripts 1 and 2 are, respectively, the indices of the first and second layer. The nearest-neighbor hopping integral on the same layer is indicated by γ_0 (2.598 eV). The four important interlayer interactions[8] used in this work are γ_1 (0.364 eV), γ_3 (0.319 eV), γ_4 (0.177 eV), and γ_6 (−0.026 eV), indicated in Figure 5a. The γ_6 is the difference of site energy between the *A* and *B* atoms owing to the interlayer coupling. The perpendicular uniform magnetic field induces a periodic Peierls phase related to the vector potential $\mathbf{A} = (0, B_0x, 0)$. The primitive unit cell shown in Figure 5b is enlarged under this periodic condition and owns four effective sublattices including $2R_B$ A_1, $2R_B$ B_1, $2R_B$ A_2, and $2R_B$ B_1 atoms. R_B is related to the dimension of the Hamiltonian under a magnetic field;[12] for example, R_B is 7900 for $B_0 = 10$ T. That is to say, each LL is the linear combination of the four magnetic TB functions associated with the four effective sublattices. The representation $A_{i,N}$ ($B_{i,N}$) indicates the *N*th ($N = 1, 2 \ldots 0.2R_B$) *A* (*B*) atom on the *i*th ($i = 1, 2$) layer. The Hamiltonian matrix elements in the presence of a magnetic field are

$$\langle \mathbf{R}_{i,N}|H_B|\mathbf{R}_{i',N'}\rangle = \gamma_s(\mathbf{R}_{i,N},\mathbf{R}_{i',N'}) \sum \frac{1}{N}\exp\left[i\mathbf{k}\cdot(\mathbf{R}_{i',N'} - \mathbf{R}_{i,N}) + i\frac{e}{\hbar}\Delta G(\mathbf{R}_{i,N},\mathbf{R}_{i',N'})\right] \quad (5)$$

where $\mathbf{R}_{i,N}$ is the position vector of $A_{i,N}$ or $B_{i,N}$. The γ_s's ($\mathbf{R}_{i,N}$, $\mathbf{R}_{i',N'}$) indicate the atomic interactions between the atoms at $\mathbf{R}_{i,N}$ and $\mathbf{R}_{i',N'}$; that is, they are γ_0, γ_1, γ_3, γ_4, and γ_6. $\Delta G(\mathbf{R}_{i,N}, \mathbf{R}_{i',N'}) = \int_0^1(\mathbf{R}_{i',N'} - \mathbf{R}_{i,N}) \times \mathbf{A}[\mathbf{R}_{i',N'} + \lambda(\mathbf{R}_{i',N'} - \mathbf{R}_{i,N})]d\lambda$ is the Peierls phase induced by a magnetic field. (Please see more detailed definitions of the Hamiltonian matrix elements in ref 12.) After diagonalizing the Hamiltonian matrix, the eigenvalues are obtained, and thus, the optical absorption function in eq 3 can be solved through gradient approximation.

Acknowledgment. This work was supported by the NSC and NCTS of Taiwan, under Grant Nos. NSC 95-2112-M-006-028-MY3 and NSC 97-2112-M-110-001-MY2.

Supporting Information Available: Influences of the interlayer interactions on the magneto-electronic and magneto-optical properties (Figures S1 and S2), Landau level and magneto-optical absorption spectra calculated with four sets of parameters (Figures S3 and S4), optical excitations obtained with four broadening parameters (Figure S5), and electronic structures and optical absorption spectra (Figures S6 and S7) of AA-stacked bilayer graphene. This material is available free of charge *via* the Internet at http://pubs.acs.org.

REFERENCES AND NOTES

1. Novoselov, K. S.; Geim, A. K.; Morozov, S. V.; Jiang, D.; Zhang, Y.; Dubonos, S. V.; Firsov, A. A. Electric Field Effect in Atomically Thin Carbon Films. *Science* **2004**, *306*, 666.
2. Novoselov, K. S.; Geim, A. K.; Morozov, S. V.; Jiang, D.; Katsnelson, M. I.; Grigorieva, I. V.; Dubonos, S. V.; Firsov, A. A. Two-Dimensional Gas of Massless Dirac Fermions in Graphene. *Nature* **2005**, *438*, 197–200.
3. Berger, C.; Song, Z. M.; Li, T. B.; Li, X. B.; Ogbazghi, A. Y.; Feng, R.; Dai, Z. T.; Marchenkov, A. N.; Conrad, E. H.; First, P. N.; de Heer, W. A. Ultrathin Epitaxial Graphite: 2D Electron Gas Properties and a Route toward Graphene-Based Nanoelectronics. *J. Phys. Chem. B* **2004**, *108*, 19912–19916.
4. Rutter, G. M.; Crain, J. N.; Guisinger, N. P.; Li, T.; First, P. N.; Stroscio, J. A. Scattering and Interference in Epitaxial Graphene. *Science* **2007**, *317*, 219–222.
5. Wallace, P. R. The Band Theory of Graphite. *Phys. Rev.* **1947**, *71*, 622–634.
6. Grüneis, A.; Attaccalite, C.; Wirtz, L.; Shiozawa, H.; Saito, R.; Pichler, T.; Rubio, A. Tight-Binding Description of the Quasiparticle Dispersion of Graphite and Few-Layer Graphene. *Phys. Rev. B* **2008**, *78*, 205425.
7. Slonczewski, J. C.; Weiss, P. R. Band Structure of Graphite. *Phys. Rev.* **1958**, *109*, 272–279.
8. Charlier, J.-C.; Michenaud, J.-P. First-Principles Study of the Electronic Properties of Simple Hexagonal Graphite. *Phys. Rev. B* **1992**, *46*, 4531–4539.
9. Latil, S.; Henrard, L. Charge Carriers in Few-Layer Graphene Films. *Phys. Rev. Lett.* **2006**, *97*, 036803.
10. Partoens, B.; Peeters, F. M. From Graphene to Graphite: Electronic Structure around the K Point. *Phys. Rev. B* **2006**, *74*, 075404.
11. Lu, C. L.; Chang, C. P.; Huang, Y. C.; Chen, R. B.; Lin, M. F. Influence of an Electric Field on the Optical Properties of Few-Layer Graphene with AB Stacking. *Phys. Rev. B* **2006**, *73*, 144427.
12. Lai, Y. H.; Ho, J. H.; Chang, C. P.; Lin, M. F. Magnetoelectronic Properties of Bilayer Bernal Graphene. *Phys. Rev. B* **2008**, *77*, 085426.
13. McCann, E.; Fal'ko, V. I. Landau-Level Degeneracy and Quantum Hall Effect in a Graphite Bilayer. *Phys. Rev. Lett.* **2006**, *96*, 086805.
14. Abergel, D. S. L.; Fal'ko, V. I. Optical and Magneto-Optical Far-Infrared Properties of Bilayer Graphene. *Phys. Rev. B* **2007**, *75*, 155430.
15. Charlier, J.-C.; Gonze, X.; Michenaud, J.-P. First-Principles Study of the Electronic Properties of Graphite. *Phys. Rev. B* **1991**, *43*, 4579–4589.
16. Nakao, J. Landau Level Structure and Magnetic Breakthrough in Graphite. *J. Phys. Soc. Jpn.* **1976**, *40*, 761–768.
17. Kuzmenko, A. B.; Crassee, I.; van der Marel, D. Determination of the Gate-Tunable Band Gap and Tight-Binding Parameters in Bilayer Graphene Using Infrared Spectroscopy. *Phys. Rev. B* **2009**, *80*, 165406.
18. Ohta, T.; Bostwick, A.; Seller, T.; Horn, K.; Rotenberg, E. Controlling the Electronic Structure of Bilayer Graphene. *Science* **2006**, *313*, 951–954.
19. Ohta, T.; Bostwick, A.; McChesney, J. L.; Seyller, T.; Horn, K.; Rotenberg, E. Interlayer Interaction and Electronic Screening in Multilayer Graphene Investigated with Angle-Resolved Photoemission Spectroscopy. *Phys. Rev. Lett.* **2007**, *98*, 206802.
20. Novoselov, K. S.; McCann, E.; Morozov, S. V.; Fal'ko, V. I.; Katsnelson, M. I.; Zeitler, U.; Jiang, D.; Schedin, F.; Geim, A. K. Unconventional Quantum Hall Effect and Berry's Phase of 2π in Bilayer Graphene. *Nat. Phys.* **2006**, *2*, 177–180.
21. Zhang, Y.; Tan, Y.-W.; Stormer, H. L.; Kim, P. Experimental Observation of the Quantum Hall Effect and Berry's Phase in Graphene. *Nature* **2005**, *438*, 201–204.
22. Miller, D. L.; Kubista, K. D.; Rutter, G. M.; Ruan, M.; de Heer, W. A.; First, P. N.; Stroscio, J. A. Observing the Quantization of Zero Mass Carriers in Graphene. *Science* **2009**, *324*, 924–927.
23. Li, G.; Andrei, E. Y. Observation of Landau Levels of Dirac Fermions in Graphite. *Nat. Phys.* **2007**, *3*, 623–627.
24. Matsui, T.; Kambara, H.; Niimi, Y.; Tagami, K.; Tsukada, M.; Fukuyama, H. STS Observations of Landau Levels at Graphite Surfaces. *Phys. Rev. Lett.* **2005**, *94*, 226403.
25. Deacon, R. S.; Chuang, K.-C.; Nicholas, R. J.; Novoselov, K. S.; Geim, A. K. Cyclotron Resonance Study of the Electron and Hole Velocity in Graphene Monolayers. *Phys. Rev. B* **2007**, *76*, 081406.

26. Henriksen, E. A.; Jiang, Z.; Tung, L.-C.; Schwartz, M. E.; Takita, M.; Wang, Y.-J.; Kim, P.; Stormer, H. L. Cyclotron Resonance in Bilayer Graphene. *Phys. Rev. Lett.* **2008**, *100*, 087403.
27. McClure, J. W. Diamagnetism of Graphite. *Phys. Rev.* **1956**, *104*, 666–671.
28. Zheng, Y.; Ando, T. Hall Conductivity of a Two-Dimensional Graphite System. *Phys. Rev. B* **2002**, *65*, 245420.
29. Ho, J. H.; Lai, Y. H.; Chiu, Y. H.; Lin, M. F. Landau Levels in Graphene. *Physica E* **2008**, *40*, 1722–1725.
30. Koshino, M.; Ando, T. Magneto-Optical Properties of Multilayer Graphene. *Phys. Rev. B* **2008**, *77*, 115313.
31. Sadowski, M. L.; Martinez, G.; Potemski, M.; Berger, C.; de Heer, W. A. Landau Level Spectroscopy of Ultrathin Graphite Layers. *Phys. Rev. Lett.* **2006**, *97*, 266405.
32. Plochocka, P.; Faugeras, C.; Orlita, M.; Sadowski, M. L.; Martinez, G.; Potemski, M.; Goerbig, M. O.; Fuchs, J.-N.; Berger, C.; de Heer, W. A. High-Energy Limit of Massless Dirac Fermions in Multilayer Graphene Using Magneto-Optical Transmission Spectroscopy. *Phys. Rev. Lett.* **2008**, *100*, 087401.
33. Benfatto, L.; Sharapov, S. G.; Carbotte, J. P. Robustness of the Optical Conductivity Sum Rule in Bilayer Graphene. *Phys. Rev. B* **2008**, *77*, 125422.
34. Nicol, E. J.; Carbotte, J. P. Optical Conductivity of Bilayer Graphene with and without an Asymmetry Gap. *Phys. Rev. B* **2008**, *77*, 155409.
35. Mucha-Kruczyński, M.; Abergel, D. S. L.; McCann, E.; Fal'ko, V. I. On Spectral Properties of Bilayer Graphene: The Effect of an SiC Substrate and Infrared Magneto-Spectroscopy. *J. Phys.: Condens. Matter* **2009**, *21*, 344206.
36. Mucha-Kruczyński, M.; McCann, E.; Fal'ko, V. I. The Influence of Interlayer Asymmetry on The Magnetospectroscopy of Bilayer Graphene. *Solid State Commun.* **2009**, *149*, 1111–1116.
37. Chang, C. P.; Lu, C. L.; Shyu, F. L.; Chen, R. B.; Fang, Y. K.; Lin, M. F. Magnetoelectronic Properties of a Graphite Sheet. *Carbon* **2004**, *42*, 2975–2980.
38. Chiu, Y. H.; Lai, Y. H.; Ho, J. H.; Chuu, D. S.; Lin, M. F. Electronic Structure of a Two-Dimensional Graphene Monolayer in a Spatially Modulated Magnetic Field: Peierls Tight-Binding Model. *Phys. Rev. B* **2008**, *77*, 045407.
39. Ho, J. H.; Lai, Y. H.; Chiu, Y. H.; Lin, M. F. Modulation Effects on Landau Levels in a Monolayer Graphene. *Nanotechnology* **2008**, *19*, 035712.
40. Huang, Y. C.; Chang, C. P.; Lin, M. F. Magnetic and Quantum Confinement Effects on Electronic and Optical Properties of Graphene Ribbons. *Nanotechnology* **2007**, *18*, 495401.
41. Chiu, Y. H.; Ho, J. H.; Chang, C. P.; Chuu, D. S.; Lin, M. F. Low-Frequency Magneto-Optical Excitations of a Graphene Monolayer: Peierls Tight-Binding Model and Gradient Approximation Calculation. *Phys. Rev. B* **2008**, *78*, 245411.
42. Huang, Y. C.; Lin, M. F.; Chang, C. P. Landau Levels and Magneto-Optical Properties of Graphene Ribbons. *J. Appl. Phys.* **2008**, *103*, 073709.
43. Lin, M. F.; Shung, K. W.-K. Plasmons and Optical Properties of Carbon Nanotubes. *Phys. Rev. B* **1994**, *50*, 17744–17747.
44. Johnson, J. G.; Dresselhaus, G. Optical Properties of Graphite. *Phys. Rev. B* **1979**, *7*, 2275–2285.
45. Chuang, K.-C.; Baker, A. M. R.; Nicholas, R. J. Magnetoabsorption Study of Landau Levels in Graphite. *Phys. Rev. B* **2009**, *80*, 161410(R).
46. Ho, Y. H.; Chiu, Y. H.; Lin, M. F. Unpublished results.